

# Non-instantaneous optical nonlinearity of an a-Si:H nanowire waveguide

Jeremiah J. Wathen,<sup>1,2,\*</sup> Vincent R. Pagán,<sup>1,3</sup> Ryan J. Suess,<sup>3,4</sup>  
Ke-Yao Wang,<sup>5</sup> Amy C. Foster<sup>5</sup> and Thomas E. Murphy<sup>1,3,4</sup>

<sup>1</sup>Laboratory for Physical Sciences, College Park, MD 20740, USA

<sup>2</sup>Department of Physics, University of Maryland, College Park, MD 20742, USA

<sup>3</sup>Department of Electrical & Computer Engineering, University of Maryland, College Park, MD 20742, USA

<sup>4</sup>Institute for Research in Electronics & Applied Physics, University of Maryland, College Park, MD 20742, USA

<sup>5</sup>Department of Electrical & Computer Engineering, Johns Hopkins University, Baltimore, Maryland 21218, USA

\*[wathenjj@lps.umd.edu](mailto:wathenjj@lps.umd.edu)

**Abstract:** We use pump-probe spectroscopy and continuous wave cross-phase and cross-amplitude modulation measurements to study the optical nonlinearity of a hydrogenated amorphous silicon (a-Si:H) nanowire waveguide, and we compare the results to those of a crystalline silicon waveguide of similar dimensions. The a-Si:H nanowire shows essentially zero instantaneous two-photon absorption, but it displays a strong, long-lived non-instantaneous nonlinearity that is both absorptive and refractive. Power scaling measurements show that this non-instantaneous nonlinearity in a-Si:H scales as a third-order nonlinearity, and the refractive component possesses the opposite sign to that expected for free-carrier dispersion.

© 2014 Optical Society of America

**OCIS codes:** (160.4330) Nonlinear optical materials; (190.4360) Nonlinear optics, devices; (190.4390) Nonlinear optics, integrated optics; (190.4720) Optical nonlinearities of condensed matter; (230.4320) Nonlinear optical devices; (230.7370) Waveguides.

---

## References and links

1. A. Harke, M. Krause, and J. Mueller, "Low-loss singlemode amorphous silicon waveguides," *Electron. Lett.* **41**, 1377–1379 (2005).
2. Y. Shoji, T. Ogasawara, T. Kamei, Y. Sakakibara, S. Suda, K. Kintaka, H. Kawashima, M. Okano, T. Hasama, H. Ishikawa, and M. Mori, "Ultrafast nonlinear effects in hydrogenated amorphous silicon wire waveguide," *Opt. Express* **18**, 5668–5673 (2010).
3. K. Narayanan and S. F. Preble, "Optical nonlinearities in hydrogenated-amorphous silicon waveguides," *Opt. Express* **18**, 8998–9005 (2010).
4. B. Kuyken, S. Clemmen, S. K. Selvaraja, W. Bogaerts, D. Van Thourhout, P. Emplit, S. Massar, G. Roelkens, and R. Baets, "On-chip parametric amplification with 26.5 dB gain at telecommunication wavelengths using CMOS-compatible hydrogenated amorphous silicon waveguides," *Opt. Lett.* **36**, 552–554 (2011).
5. B. Kuyken, H. Ji, S. Clemmen, S. K. Selvaraja, H. Hu, M. Pu, M. Galili, P. Jeppesen, G. Morthier, S. Massar, L. K. Oxenløwe, G. Roelkens, and R. Baets, "Nonlinear properties of and nonlinear processing in hydrogenated amorphous silicon waveguides," *Opt. Express* **19**, B146–B153 (2011).
6. C. Lacava, P. Minzioni, E. Baldini, L. Tartara, J. M. Fedeli, and I. Cristiani, "Nonlinear characterization of hydrogenated amorphous silicon waveguides and analysis of carrier dynamics," *Appl. Phys. Lett.* **103**, 141103 (2013).
7. J. Matres, G. C. Ballesteros, P. Gautier, J.-M. Fédéli, J. Martí, and C. J. Oton, "High nonlinear figure-of-merit amorphous silicon waveguides," *Opt. Express* **21**, 3932–3940 (2013).

8. C. Grillet, L. Carletti, C. Monat, P. Grosse, B. Ben Bakir, S. Menezo, J. M. Fedeli, and D. J. Moss, "Amorphous silicon nanowires combining high nonlinearity, FOM and optical stability," *Opt. Express* **20**, 22609–22615 (2012).
9. J. S. Pelc, K. Rivoire, S. Vo, C. Santori, D. A. Fattal, and R. G. Beausoleil, "Picosecond all-optical switching in hydrogenated amorphous silicon microring resonators," *Opt. Express* **22**, 3797–3810 (2014).
10. K.-Y. Wang and A. C. Foster, "Ultralow power continuous-wave frequency conversion in hydrogenated amorphous silicon waveguides," *Opt. Lett.* **37**, 1331–1333 (2012).
11. S. Suda, K. Tanizawa, Y. Skakakibara, T. Kamei, K. Nakanishi, E. Itoga, T. Ogasawara, R. Takei, H. Kawashima, S. Namiki, M. Mori, T. Hasama, and H. Ishikawa, "Pattern-effect-free all-optical wavelength conversion using a hydrogenated amorphous silicon waveguide with ultra-fast carrier decay," *Opt. Lett.* **37**, 1382–1384 (2012).
12. S. Clemmen, A. Perret, S. K. Selvaraja, D. van Thourhout, R. Baets, P. Emplit, and S. Massar, "Generation of correlated photons in hydrogenated amorphous-silicon waveguides," *Opt. Lett.* **35**, 3483–3485 (2010).
13. S. Uvin, U. D. Dave, B. Kuyken, S. Selvaraja, F. Leo, and G. Roelkens, "Mid-infrared to telecom-band stable supercontinuum generation in hydrogenated amorphous silicon waveguides," in *Proceedings of IEEE Photonics Conference (IEEE, 2013)*, pp. 380–381.
14. K. G. Petrillo, K.-Y. Wang, A. C. Foster, and M. A. Foster, "Highly sensitive ultrafast pulse characterization using hydrogenated amorphous silicon waveguides," *Opt. Express* **21**, 31229–31238 (2013).
15. K.-Y. Wang, M. A. Foster, and A. C. Foster, "Wavelength-agile near-IR chip-based optical parametric oscillator using a deposited silicon waveguide," in *CLEO: 2013 Postdeadline*, OSA Postdeadline Paper Digest (online) (Optical Society of America, 2013), paper CTh5D.7.
16. K.-Y. Wang, V. G. Velev, K. F. Lee, A. S. Kowligy, P. Kumar, M. A. Foster, A. C. Foster, and Y.-P. Huang, "Multichannel photon-pair generation using hydrogenated amorphous silicon waveguides," *Opt. Lett.* **39**, 914–916 (2014).
17. X. Gai, D.-Y. Choi, and B. Luther-Davies, "Negligible nonlinear absorption in hydrogenated amorphous silicon at 1.55  $\mu\text{m}$  for ultra-fast nonlinear signal processing," *Opt. Express* **22**, 9948–9958 (2014).
18. V. Mizrahi, K. W. DeLong, G. I. Stegeman, M. A. Saifi, and M. J. Andrejco, "Two-photon absorption as a limitation to all-optical switching," *Opt. Lett.* **14**, 1140–1142 (1989).
19. K. W. DeLong, K. B. Rochford, and G. I. Stegeman, "Effect of two-photon absorption on all-optical guided-wave devices," *Appl. Phys. Lett.* **55**, 1823–1825 (1989).
20. K.-Y. Wang and A. C. Foster, "GHz Near-IR Optical Parametric Amplifier using a Hydrogenated Amorphous Silicon Waveguide," in *CLEO: 2014*, OSA Technical Digest (online) (Optical Society of America, 2014), paper SW3L.7.
21. K. Ikeda, Y. Shen, and Y. Fainman, "Enhanced optical nonlinearity in amorphous silicon and its application to waveguide devices," *Opt. Express* **15**, 17761–17771 (2007).
22. J. J. Wathen, V. R. Pagán, and T. E. Murphy, "Simple method to characterize nonlinear refraction and loss in optical waveguides," *Opt. Lett.* **37**, 4693–4695 (2012).
23. R. J. Suess, M. M. Jadidi, K. Kim, and T. E. Murphy, "Characterization of optical nonlinearities in nanoporous silicon waveguides via pump-probe heterodyning technique," *Opt. Express* **22**, 17466–17477 (2014).
24. V. R. Almeida, R. R. Panepucci, and M. Lipson, "Nanotaper for compact mode conversion," *Opt. Lett.* **28**, 1302–1304 (2003).
25. A. B. Fallahkhair, K. S. Li, and T. E. Murphy, "Vector finite difference modesolver for anisotropic dielectric waveguides," *J. Lightwave Technol.* **26**, 1423–1431 (2008).
26. J. Cardenas, C. B. Poitras, J. T. Robinson, K. Preston, L. Chen, and M. Lipson, "Low loss etchless silicon photonic waveguides," *Opt. Express* **17**, 4752–4757 (2009).
27. R. Takei, S. Manako, E. Omoda, Y. Sakakibara, M. Mori, and T. Kamei, "Sub-1 dB/cm submicrometer-scale amorphous silicon waveguide for backend on-chip optical interconnect," *Opt. Express* **22**, 4779–4788 (2014).
28. F. Devaux, Y. Sorel, and J. F. Kerdiles, "Simple measurement of fiber dispersion and of chirp parameter of intensity modulated light emitter," *J. Lightwave Technol.* **11**, 1937–1940 (1993).
29. M. Dinu, F. Quochi, and H. Garcia, "Third-order nonlinearities in silicon at telecom wavelengths," *Appl. Phys. Lett.* **82**, 2954–2956 (2003).
30. A. R. Motamedi, A. H. Nejadmalayeri, A. Khilo, F. X. Kärtner, and E. P. Ippen, "Ultrafast nonlinear optical studies of silicon nanowaveguides," *Opt. Express* **20**, 4085–4101 (2012).

---

## 1. Introduction

Hydrogenated amorphous silicon (a-Si:H) is a promising material for optical processing in integrated silicon photonics. Films of a-Si:H can be deposited at low temperatures (in the range of 250 to 400°C) using plasma-enhanced chemical vapor deposition (PECVD), which means the material is back-end-of-the-line compatible with standard complementary-metal-oxide-semiconductor (CMOS) fabrication techniques. As a depositable waveguide material,

a-Si:H poses the possibility of easy on-chip vertical stacking and vertical coupling of photonic structures [1].

Over the past several years, many groups have studied the nonlinear properties of a-Si:H in waveguide geometries [1–17]. The suitability of a waveguide for nonlinear optical processes is usually characterized by its nonlinear figure-of-merit (FOM), which is composed of the ratio of the real part to the imaginary part of its third-order nonlinear susceptibility [18]. We follow the convention  $\text{FOM} \equiv \gamma_R / (4\pi\gamma_I)$ , where  $\gamma$  is the waveguide's complex nonlinear parameter given by  $\gamma = \gamma_R + i\gamma_I = \frac{1}{A_{\text{eff}}} \left( \frac{\omega n_2}{c} + i\frac{\alpha_2}{2} \right)$ ,  $A_{\text{eff}}$  is the effective mode area,  $\omega$  is the optical frequency, and  $n_2$  and  $\alpha_2$  represent the material's instantaneous Kerr coefficient and two-photon-absorption (2PA) coefficient, respectively. A large FOM, meaning a small proportion of nonlinear absorption compared to nonlinear refraction, is typically desirable for all-optical processing applications [19].

Because a-Si:H has been reported to have a quasi-bandgap of  $\sim 1.7$  eV, which is larger than the two-photon energy at telecommunications wavelengths, it should exhibit small two-photon absorption compared to crystalline silicon (c-Si). However, in contrast to c-Si, the nonlinear characteristics of a given specimen of a-Si:H depend strongly on the fabrication conditions. Presumably, the extent of disorder in the amorphous silicon and the extent to which hydrogen atoms terminate dangling bonds impact the amount of nonlinear absorption, though a cause-and-effect relationship between fabrication conditions and the nonlinear traits of a-Si:H has yet to be established. Published values of the FOM for a-Si:H waveguides span a broad range, including 0.4 [2], 0.66 [3], 2.1 [4, 5], 3.06 [6], 4.9 [7], and 5 [8]. Nonetheless, a-Si:H waveguides have recently been used in an exciting array of applications, including all-optical switching [9], wavelength conversion [10, 11], correlated pair generation [12, 16], supercontinuum generation [13], high-speed waveform sampling [5], ultrafast pulse characterization [14], on-chip net parametric gain [4, 20] and wavelength-agile optical parametric oscillation [15].

However, as conventionally defined, the FOM is related only to the instantaneous nonlinear properties. Even with a large FOM, a waveguide can demonstrate a non-instantaneous nonlinearity that can significantly limit the efficiency of nonlinear signal processing. For example, in crystalline silicon, free-carrier absorption severely impairs the performance of many nonlinear devices. Thus, understanding the nature of the non-instantaneous nonlinearity in a-Si:H is crucial to engineering future photonic devices from this promising material. On this topic, it is important to point out that in crystalline silicon devices, the effects of free carriers can at least be mitigated through the incorporation of p–n junctions. At present, this degree of freedom has not been demonstrated for devices composed of hydrogenated amorphous silicon, a fact which further highlights the need to understand the non-instantaneous nonlinearity in a-Si:H.

Unfortunately, reports of the non-instantaneous nonlinearity in a-Si:H vary considerably, and a generally accepted model to describe the non-instantaneous behavior has yet to emerge. Ikeda et al. published one of the first studies of the third-order nonlinearity in a-Si:H [21]. They performed side-by-side z-scan measurements on thin samples of non-hydrogenated amorphous silicon (a-Si), a-Si:H, c-Si and SiO<sub>2</sub>. Noting that the closed-aperture z-scan for a-Si was inverted with respect to that for SiO<sub>2</sub>, the authors concluded that the dominant nonlinearity in a-Si (and, by extension, a-Si:H) must be non-instantaneous refraction and absorption from a long-lived free-carrier plasma. Additionally, their open-aperture z-scan measurements showed that the a-Si and a-Si:H samples displayed very large nonlinear absorption in comparison to c-Si, despite having a larger bandgap. To explain the combination of enhanced nonlinear absorption and the presumed free-carrier refractive nonlinearity, the authors constructed a model in which free carriers were generated via “two-step” or “two-state” absorption (TSA). In the TSA model, they assumed that sequential one-photon absorptions, facilitated by mid-gap electronic states, generated free carriers at an enhanced rate relative to what might be expected from 2PA alone.

However, other groups have disputed the applicability of the TSA model to describe their a-Si:H samples. For example, Narayanan and Preble [3] conducted measurements of the power-dependent transmission of short pulses through an a-Si:H waveguide, and they attributed the nonlinear transmission to a combination of 2PA and FCA, as in crystalline silicon. Likewise, Kuyken et al. [5] and Lacava et al. [6] relied on the 2PA+FCA model to explain their transient nonlinear absorption measurements.

One very thorough method for characterizing the non-instantaneous nonlinearity in a waveguide is the heterodyne pump-probe measurement. This time-resolved technique is simultaneously sensitive to the phase and amplitude of the probe, and can distinguish between cross-amplitude modulation (XAM) and cross-phase modulation (XPM). In the first heterodyne pump-probe measurements reported on an a-Si:H waveguide [2], both the amplitude and phase of the probe demonstrated a non-instantaneous response. The non-instantaneous phase change exhibited the same sign as the instantaneous Kerr effect, opposite to the phase shift expected for free-carrier dispersion. However, the observed transient was short-lived and weak, making it difficult to draw definite conclusions about the non-instantaneous nonlinearity in their waveguide. In contrast, in a more recent heterodyne pump-probe measurement of an a-Si:H waveguide [7], essentially no non-instantaneous nonlinear absorption and refraction were observed.

In this work, we present a systematic study of the non-instantaneous nonlinearity of an a-Si:H nanowire waveguide using several experimental techniques. The waveguide we study is similar to the one presented in [10] and [15]. For comparison, we conduct the same experiments on a c-Si nanowire of comparable dimensions. The experiments include: (1) a modified version of the nonlinear loss tangent experiment described in [22]; (2) a phase-insensitive transient absorption experiment using a CW probe and pulsed pump, similar to those in [5] and [6]; and (3) a two-frequency heterodyne pump-probe experiment described in [23]. Taken together, our experiments show that the a-Si:H waveguide demonstrates essentially zero instantaneous nonlinear absorption, but it does exhibit appreciable non-instantaneous nonlinear absorption and refraction. Moreover, we observe that the non-instantaneous amplitude transient in this waveguide scales in direct proportion to the applied pump power, indicating the non-instantaneous nonlinearity is effectively a third-order nonlinearity rather than a combination of instantaneous two-photon absorption followed by free-carrier absorption. Finally, our measurements show that the non-instantaneous nonlinear refraction has the same sign as the instantaneous Kerr refraction, which cannot be attributed to the dispersive effect of free carriers.

## 2. The a-Si:H and c-Si nanowires

The a-Si:H nanowire was fabricated by PECVD deposition of an a-Si:H film onto a silicon wafer, which has a 3- $\mu\text{m}$  thermal oxide layer. In the a-Si:H film deposition chamber, a gas flow of 1200 sccm made up of helium with 5% silane was kept at a pressure of 900 mT with 50 W RF power. The substrate was maintained at approximately 300°C for low-temperature deposition. A layer of silicon dioxide was deposited as a hard mask to reduce effects from direct etching with organic resists. Electron beam lithography followed by chlorine-based inductively coupled plasma (ICP) etching was used for waveguide patterning. Inverse adiabatic tapers on both ends of the waveguide were made for optical coupling [24]. The a-Si:H core layer is 215 nm thick and 600 nm wide. A 1- $\mu\text{m}$ -thick SiO<sub>2</sub> layer was deposited over the waveguide via PECVD for an optical cladding. The c-Si waveguide was fabricated on a SOI (silicon-on-insulator) platform with a 3- $\mu\text{m}$  buried oxide. The same patterning techniques were used and the waveguide has similar dimensions: 270 nm thick and 620 nm wide, with a 1- $\mu\text{m}$  SiO<sub>2</sub> cladding.

In all the experiments presented here, only the transverse-electric (TE) eigenmode of the waveguide is excited. The TE eigenmodes were calculated using the finite difference method

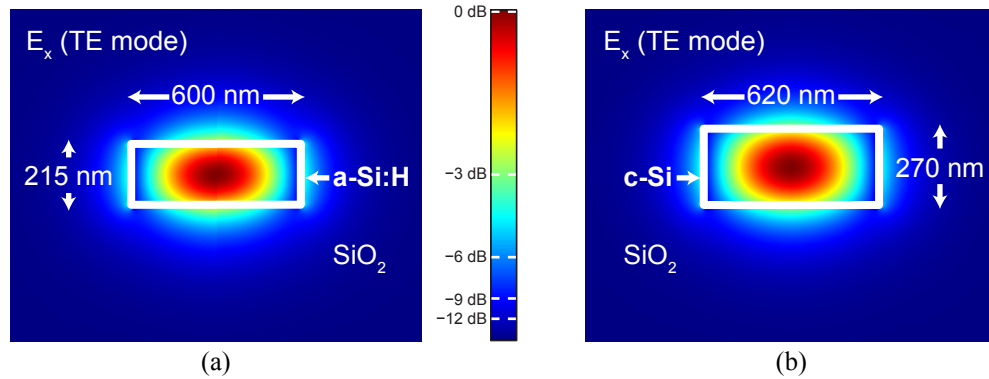


Fig. 1. False-color images of the calculated mode for (a) the a-Si:H nanowire and (b) the c-Si nanowire. The images show the magnitude of the x-component of the electric field for the TE eigenstate.

[25], and are shown in Fig. 1 with overlays to indicate the cross-sectional composition of each waveguide. Both nanowire waveguides are 1 cm long and have a linear loss of approximately 3 dB/cm, measured using the cutback technique.

We acknowledge that the two waveguides have slightly different cross-sectional dimensions and the propagation losses are not quite state-of-the-art [26, 27]. However, the differences between the cross-sections and the less-than-ideal propagation losses will not change the overall characteristics of the non-instantaneous nonlinearities, which we compare in the following analysis.

### 3. Nonlinear loss tangent measurements

The measurements presented in this section were made using variants of the experimental technique described in [22]. The method was first developed to make a direct measurement of a waveguide's nonlinear loss tangent, which is essentially the inverse of the FOM presented in the introduction:  $\tan \phi \equiv \gamma_I / \gamma_R = (4\pi \times \text{FOM})^{-1}$ . (The FOMs of the various a-Si:H waveguides listed in the introduction translate to  $\tan \phi = 0.2$  [2], 0.12 [3], 0.038 [4, 5], 0.026 [6], 0.016 [7], and 0.015 [8].)

The experimental setup is depicted in Fig. 2. A Mach-Zehnder modulator imparts a sinu-

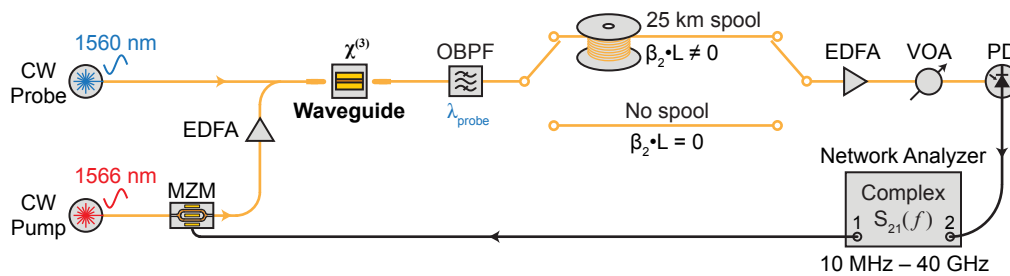


Fig. 2. The experimental setup used to measure the nonlinear properties of the nanowires. The setup is shown with and without an optional spool of dispersive fiber. CW: continuous-wave; EDFA: erbium-doped fiber amplifier; MZM: Mach-Zehnder modulator; OBPF: optical bandpass filter; VOA: variable optical attenuator; PD: high-speed photodiode.

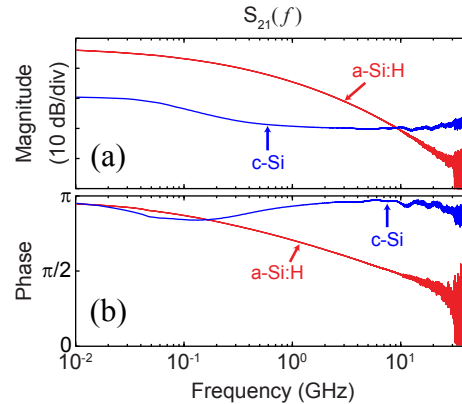


Fig. 3. (a) Magnitude and (b) phase of  $S_{21}$  vs. the modulation frequency for the case with no dispersive fiber in the setup. Red traces represent the a-Si:H nanowire while blue traces represent the c-Si nanowire.

sinusoidal intensity modulation to a strong CW pump beam. The pump is combined with a weak CW probe, and the co-polarized beams are launched into the waveguide's TE eigenmode using a polarization-maintaining (PM) lensed optical fiber. The fiber-to-waveguide coupling was estimated to be  $-8$  dB for the c-Si and a-Si:H waveguides, and in both cases approximately 25 mW of pump power and 1 mW of probe power were launched into the waveguide. In the waveguide, the sinusoidal modulation of the pump is transferred to the probe via a combination of XAM and XPM. Following the waveguide, an optical bandpass filter suppresses the pump, and the probe is passed through an optional 25-km spool of dispersive single-mode fiber (SMF). When the SMF spool is installed in the setup, the dispersion of the fiber converts intensity modulation to phase modulation and vice versa in a manner that depends on the frequency of the modulation [28]. The probe is amplified by an EDFA before detection in a 65-GHz square-law photoreceiver. The photocurrent is received by a network analyzer, which sweeps the modulation frequency from 10 MHz to 40 GHz and records the system's complex  $S_{21}$  transfer function.

We first consider the experiments conducted without the spool of fiber installed in the setup. In this configuration, the measurement characterizes the cross-amplitude modulation (XAM) as a function of modulation frequency. As shown in the blue traces of Fig. 3(a), the crystalline silicon waveguide shows 10 dB higher cross-amplitude modulation at frequencies below approximately 50 MHz, but reaches a plateau at higher frequencies. Apart from a small dip near this corner frequency, the phase of the  $S_{21}(f)$  measurement, shown in Fig. 3(b), asymptotically approaches  $\pi$  in both the high and low frequency limits. The phase of  $S_{21}(f)$ , which should not be confused with the optical phase of the probe wave, is an indication that the nonlinearity is absorptive: when the pump is stronger, the probe signal becomes absorbed, thereby causing their envelopes to be exactly  $\pi$  out of phase with one another. The higher XAM observed at low modulation frequencies is caused by free carrier absorption in the c-Si waveguide. The  $-3$  dB roll-off point in this curve falls at approximately  $f_c = 85$  MHz, from which we estimate the free carrier lifetime to be  $1/(2\pi f_c) = 1.9$  ns. The high-frequency plateau in the XAM spectrum is well explained by non-degenerate two-photon absorption between the pump and probe – an instantaneous absorptive nonlinear effect that occurs across all modulation frequencies.

In contrast, for the a-Si:H waveguide, the magnitude of  $S_{21}(f)$  falls monotonically with the modulation frequency, similar to the behavior of a low-pass filter. Although it was not possible to measure the asymptotic phase response beyond 40 GHz, the phase undergoes a net shift of  $-\pi/2$  over the frequency range observed, again suggesting a low-pass response. In the limit of

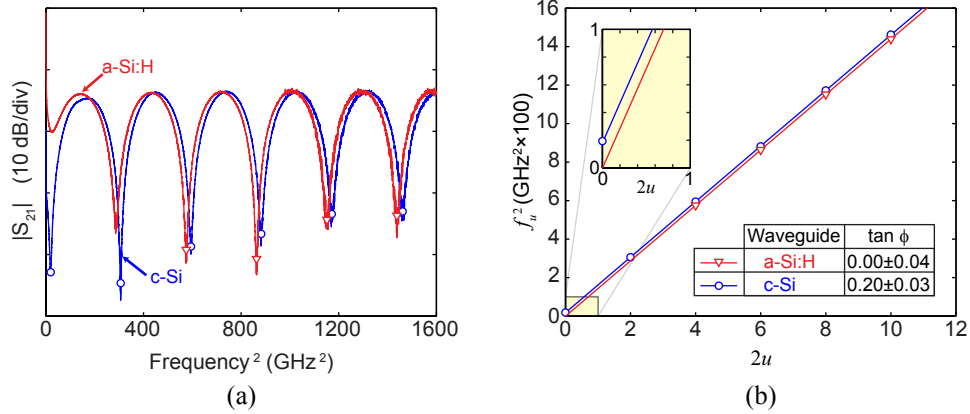


Fig. 4. (a) The magnitude of  $S_{21}$  vs. the square of the modulation frequency with dispersive fiber in the setup. (b)  $f_u^2$  vs.  $2u$  for both waveguides obtained from 10 consecutive  $S_{21}(f)$  measurements. Inset: The same linear fits for both waveguides, enlarged to show the difference in the intercepts. The nonlinear loss tangent of Eq. (2) is calculated using a linear regression of the null-frequencies, and the uncertainty is estimated using the 95% confidence bounds obtained from the least-squares fit.

low modulation frequency, the a-Si:H waveguide exhibits significantly stronger XAM than its c-Si counterpart. Yet, the absence of a high-frequency plateau in the magnitude measurement indicates that instantaneous two-photon absorption is absent or negligible for a-Si:H. Because of the apparent absence of two-photon absorption, the slower nonlinearity cannot be adequately described by free carrier absorption, as was the case for the c-Si. The  $-3$  dB roll-off point in this curve falls at approximately  $f_c = 105$  MHz, from which we estimate a corresponding lifetime of  $1/(2\pi f_c) = 1.5$  ns.

We next repeated the experiment with a 25-km spool of SMF fiber installed after the device, which permits measurement of the ratio of XAM to XPM. The group-velocity dispersion ( $D$ ) in the optical fiber of length  $L$  causes the upper and lower modulation-sidebands ( $\pm f$ ) of the probe to accumulate an additional phase of  $\pi\lambda^2 DLf^2/c$  relative to the carrier. The additional phase adds to the initial sideband phase angle,  $\phi$ , created by phase and intensity modulation in the waveguide under test. As explained in [22], the received signal will exhibit a null in the modulation transfer function at frequencies where  $\pi\lambda^2 DLf^2/c - \phi$  is an integral multiple of  $\pi$ . Figure 4(a) shows the measured magnitude of the  $S_{21}(f)$  transfer functions for both nanowire waveguides. The null-frequencies in the transfer functions are given by:

$$f_u^2 = \frac{c}{2DL\lambda^2} \left( 2u + \frac{2}{\pi}\phi \right), \quad u = 0, 1, 2, \dots \quad (1)$$

where  $f_u$  is the frequency corresponding to the  $u^{\text{th}}$  null,  $c$  is the speed of light,  $DL$  is the fiber's dispersion-length product, and  $\lambda$  is the probe's wavelength. In this expression, the quantity  $\phi$  is related to the waveguide's nonlinear loss tangent,

$$\tan \phi = \frac{\gamma_I}{\gamma_R} = \frac{\lambda \alpha_2}{4\pi n_2} \quad (2)$$

which is a measure of the ratio of intensity to phase modulation. Provided this ratio is independent of the modulation frequency, one can determine the nonlinear loss tangent by linear regression to find the intercept points of Eq. (2), as shown in Fig. 4(b).

For the a-Si:H waveguide, the non-instantaneous nonlinearity shifts and obscures the two lowest-order nulls ( $u = 0$  and 1). But, based on the data of Fig. 3(a), the magnitude of the non-instantaneous component to the nonlinearity can be safely ignored for modulation frequencies above 20 GHz. We therefore excluded the first two nulls in order to apply Eq. (1), which was derived under the assumption of a purely instantaneous nonlinearity. By considering only the high-frequency asymptotic behavior, we thereby obtain an estimate of the instantaneous nonlinear loss tangent. As shown in Fig. 4(b), we fit the null-frequencies for  $u = 2$  through 5 to a straight line to obtain the slope and intercept of Eq. (1). The fit yields  $\tan \phi = 0.00 \pm 0.04$ , which confirms the absence of instantaneous nonlinear absorption in the a-Si:H waveguide. For c-Si, the non-instantaneous nonlinear absorption is relatively insignificant compared to the instantaneous effects, so we chose to include all of the nulls ( $u = 0$  through 5) in the fitting procedure. We obtain  $\tan \phi = 0.20 \pm 0.03$ , which is in good agreement with published values for bulk c-Si [29].

#### 4. Transient absorption using a CW probe

The experimental setup used to measure transient absorption in the nanowires is depicted in Fig. 5. A passively mode-locked fiber laser (MLL) produces hyperbolic-secant-squared pump pulses with a pulsewidth of 2 ps. The repetition rate of the pump laser is 10 MHz, and the center-wavelength is 1530 nm. A separate external cavity laser produces the CW probe at 1560 nm. The co-polarized pump and probe are combined and launched into the TE eigenstate of the waveguide using a PM lensed fiber. A 5% power tap just prior to the lensed fiber monitors the pump and probe powers. The fiber-to-waveguide coupling loss for both waveguides is about 8 dB. For all the experiments presented in this section, the probe power coupled into the waveguide was 1 mW, and the power of the pump was adjusted using a variable optical attenuator to observe the scaling of the transient absorption with pump power. The highest achievable peak power of the pump pulses was about 8.4 W in the input lensed fiber, or about 1.3 W of peak power into the waveguide. At the output of the waveguide, the pump is suppressed using optical bandpass filters and the probe is amplified by an erbium-doped fiber amplifier. The probe is detected using a 65-GHz photodiode, and the transient absorption response is recorded on a 30-GHz digital sampling oscilloscope.

The transient absorption data for the a-Si:H and c-Si waveguides are shown in Figs. 6(a) and 6(b), respectively. We collected data over a time-window of 100 ns (the full inter-pulse interval). However, to emphasize the scaling of the transients close to  $t = 0$ , Figs. 6(a) and 6(b)

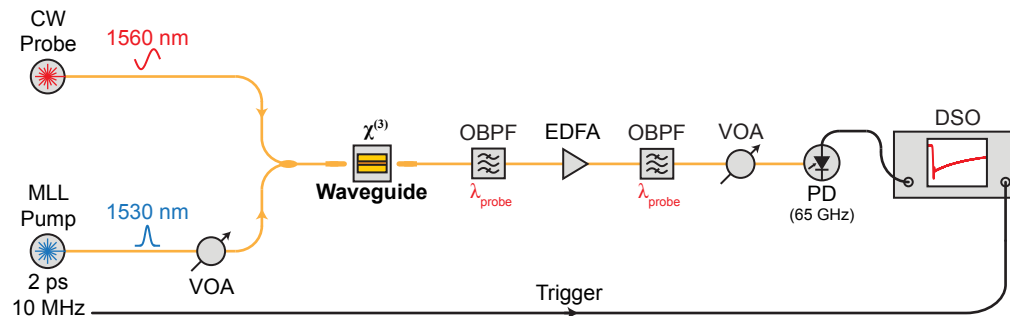


Fig. 5. The experimental setup used to measure transient nonlinear absorption in the nanowires. MLL: mode-locked laser; CW: continuous wave; VOA: variable optical attenuator; OBPF: optical bandpass filter; EDFA: erbium-doped fiber amplifier; PD: high-speed photodiode; DSO: digital sampling oscilloscope.

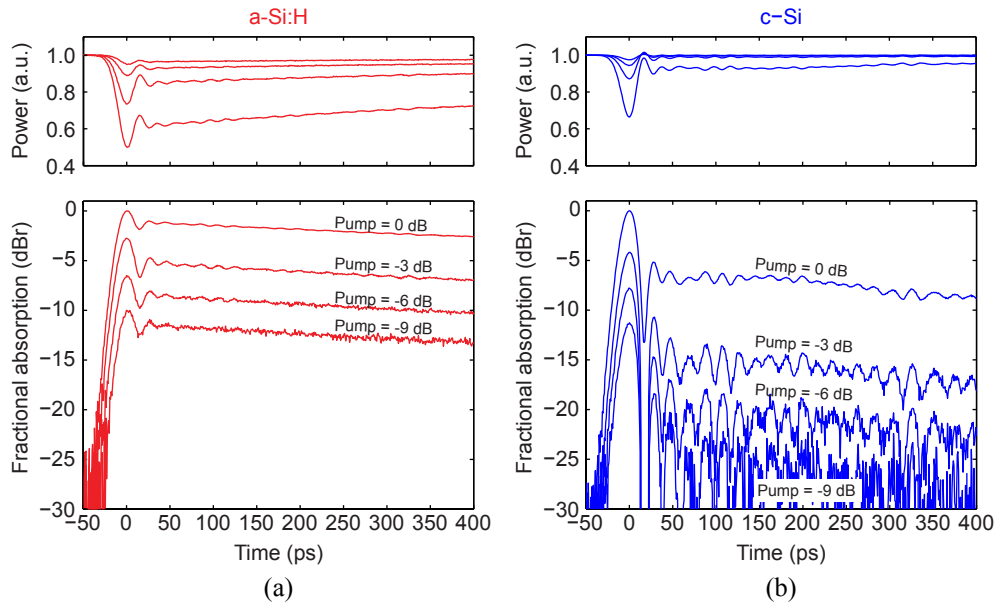


Fig. 6. Transient absorption of the probe for (a) the a-Si:H nanowire and (b) the c-Si nanowire. Top: normalized probe power vs. time. Bottom: Fractional absorption of the probe vs. time. Zero time-delay is registered to the extremum in each transient and positive time indicates time since the extremum.

only show the data through  $t = 400$  ps. The top axes in Figs. 6(a) and 6(b) show the transient absorption of the probe for four pump powers, where the pump power has been incremented in 3-dB steps. The transients are normalized to their average value prior to the arrival of the pump (i.e.,  $P(t)/P_0$ ). The bottom axes show the same data, but the normalized  $P(t)$  has been subtracted from 1 (i.e., fractional absorption =  $1 - P(t)/P_0$ ). The fractional absorption data are plotted in dBr, decibels relative to the extremum in the transient for the highest pump power. Graphing the data in this manner makes clear the scaling of the transients as a function of pump power. In these traces, the abrupt recovery at about  $t = 25$  ps and the fast ripples afterward are caused by the impulse response of the detector, which has not been deconvolved from the experimental results.

For the c-Si nanowire, the instantaneous part of the transient occurring at  $t = 0$  is distinct from the non-instantaneous recovery, and scales in direct proportion to the pump power, as expected for non-degenerate two-photon absorption. On the other hand, the long-lived, non-instantaneous portion of the transient scales approximately with the square of the pump power. This scaling behavior is well-explained by free-carrier absorption, wherein the free carrier population is created by degenerate 2PA of the pump pulses and therefore scales in proportion to  $P_{\text{pump}}^2$ . We note that the observed  $1/e$  lifetime of the c-Si transient (excluding the instantaneous portion) is approximately 2 ns, which roughly agrees with the  $S_{21}(f)$  measurements presented in Fig. 3(a).

In contrast to the c-Si result, the a-Si:H nanowire exhibits a very different scaling relationship: The entire transient response is observed to scale roughly in direct proportion to the pump power, with no clear separation between the instantaneous and non-instantaneous components. This power scaling is illustrated in Fig. 7(a), which shows the fractional absorption versus the applied power for a fixed time-delay of 400 ps. Figure 7(b) shows the fractional absorption data for the highest pump power over a time interval of 20 ns. While it cannot be described

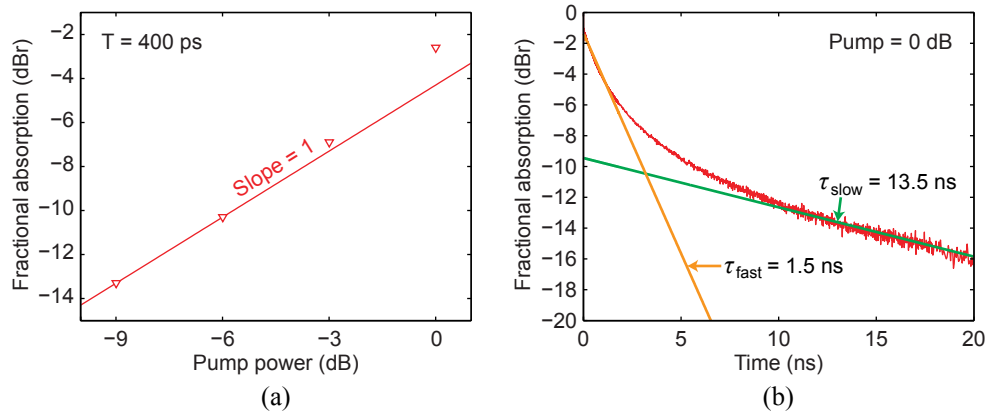


Fig. 7. (a) Fractional absorption of the probe versus the applied pump power for the a-Si:H waveguide. The solid red line is a guide for the eye. (b) Transient absorption of the probe (the same as the highest-power trace in Fig. 6(a), but the scale is adjusted to show a longer interval).

by a simple mono-exponential function, it can be divided into two regions, one dominated by a fast exponential decay (with  $\tau_{\text{fast}} = 1.5 \text{ ns}$ ) and the other by a slow exponential decay (with  $\tau_{\text{slow}} = 13.5 \text{ ns}$ ). The observed  $1/e$  response time of the a-Si:H is 1.5 ns, which agrees with the  $S_{21}(f)$  measurements presented in Fig. 3(a). However, that the transients scale linearly with pump power indicates that the non-instantaneous response cannot be attributed to free-carrier effects. A better description of the nonlinear response would be through another third-order-nonlinearity effect, perhaps related to mid-gap states or other intermediate electronic states with nanosecond lifetimes.

## 5. Heterodyne pump-probe measurements

The transient absorption measurements described in the preceding section only characterize the cross-absorption modulation between the pump and probe. To measure the phase response as well, we employed a two-frequency heterodyne pump-probe setup, depicted in Fig. 8. The details of the experimental technique are described in [23]. The pump and probe pulses are

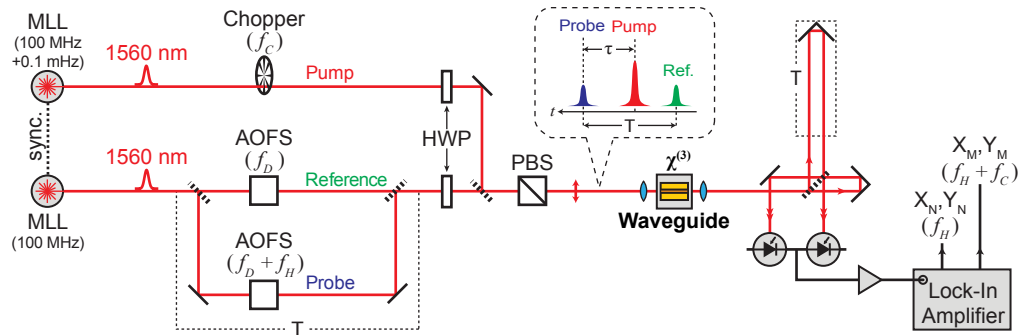


Fig. 8. The two-frequency heterodyne pump-probe experiment. The inset shows the relative timing of the reference, pump and probe pulses. MLL: mode-locked laser; AOFS: acousto-optic frequency shifter; HWP: half waveplate; PBS: polarizing beam splitter.

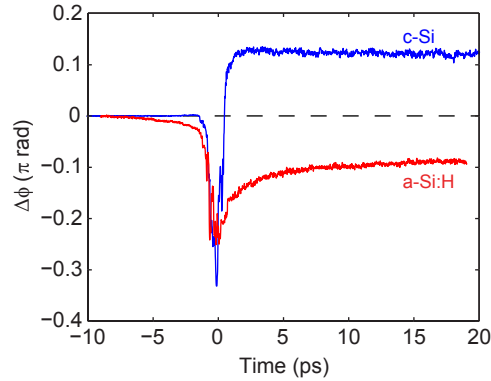


Fig. 9. Time-resolved phase transients for the a-Si:H (red) and c-Si (blue) nanowires. In these experiments, the launched pump powers were  $264 \mu\text{W}$  and  $431 \mu\text{W}$ , respectively.

produced by two electronically synchronized mode-locked fiber lasers (Menlo Systems). The pulses emitted by both lasers have a central wavelength of 1560 nm and pulsewidth of 100 fs. The first laser generates only the pump pulses, while the output of the second laser is split evenly to provide the reference and probe pulses, which precede and succeed the pump pulse, respectively. The time-offset between the probe and reference pulses is fixed at  $T = 830$  ps. The repetition rate of the probe/reference laser was fixed at 100 MHz, while the pump laser was adjusted to a rate of  $100 \text{ MHz} + 0.1 \text{ mHz}$ , which causes the time delay between the pump and probe pulses to continuously sweep at a rate of 1 ps/s.

Acousto-optic frequency shifters (AOFS) introduce a blue-shift to the probe and reference pulses. The reference pulses are up-shifted by  $f_D = 35$  MHz while the probe pulses are up-shifted by  $f_D + f_H = 35.0625$  MHz ( $f_D$  denotes the resonant drive frequency of the AOFS). The detection ultimately relies on measuring the heterodyne beat between the probe and reference, which has a frequency  $f_H = 62.5$  kHz. The pump beam is mechanically chopped at  $f_C = 1$  kHz. For a given pump-probe delay,  $\tau$ , chopping the pump allows comparison of phase and amplitude of the probe with the pump on (when the chopper wheel passes the pump) relative to the phase and amplitude of the probe with the pump off (when the chopper blade occludes the pump).

The probe/reference and pump beams pass through separate half-wave plates (used to adjust the power in each beam), and the beams are combined using a beam splitter. A polarizing beam splitter prior to the coupling optics passes only the horizontal component of the electric field, in order to excite only the TE eigenstate of the waveguide. A high-numerical-aperture aspheric lens ( $60\times$ , N.A. = 0.65) launches the light into the waveguide. In the waveguide, XAM and XPM modify the amplitude and phase of the probe as a function of the pump-probe delay. At the output of the waveguide, the light is collimated by a microscope objective, and directed into a Michelson that realigns the probe and reference pulses in time. The two complementary outputs from the interferometer are recorded using a balanced detector, which suppresses the common mode noise of the pump. A dual-phase lock-in amplifier simultaneously detects both quadratures at both the heterodyne frequency,  $f_H$ , and at the first upper sideband of the heterodyne frequency,  $f_H + f_C$ . From these two measurements, one can calculate the cross-phase modulation  $\Delta\phi$  as the time delay  $\tau$  is swept [23].

Figure 9 compares the phase transients for the a-Si:H and c-Si waveguides. We attribute the unphysical leading edge in the a-Si:H transient to a difference between the pulse-shapes used in the two experiments. For the a-Si:H experiment, we estimate the average probe power launched into the waveguide was  $0.3 \mu\text{W}$  while the average launched pump power was  $264 \mu\text{W}$ . For

the c-Si experiment, we estimate the average probe power launched into the waveguide was  $0.46 \mu\text{W}$ , while the average launched pump power was  $431 \mu\text{W}$ .

The heterodyne measurements shown in Fig. 9 reveal that the non-instantaneous amplitude transient is accompanied by a corresponding non-instantaneous phase transient, for both waveguides. The phase transient recorded for the c-Si nanowire agrees well with previously published results [30]. However, the a-Si:H waveguide is seen to behave dramatically differently from the c-Si waveguide: the non-instantaneous phase transient is positive (indicating a non-instantaneous pump-induced increase in refractive index), while for c-Si it is negative, as expected for free-carrier dispersion. This result, which confirms earlier reports from Shoji et al. [2], provides further evidence that the non-instantaneous nonlinearity in a-Si:H is not attributable to free carriers.

## 6. Discussion

Taken together, our measurements thoroughly characterize the non-instantaneous nonlinear response in this a-Si:H nanowire. Though the results we have presented do not indicate the precise microscopic origin of the delayed nonlinear response, several features emerge that are different from what is commonly observed in crystalline silicon.

First, this a-Si:H waveguide does not exhibit instantaneous two-photon absorption; this fact alone indicates free carriers are not responsible for the non-instantaneous component of the nonlinearity. The absence of instantaneous two-photon absorption is consistent with at least one earlier study of a-Si:H [17], but at odds with most previous reports [2, 3, 5–8]. On this point, it bears repetition that the optical properties of a-Si:H depend on how it is deposited and processed. Fabrication-dependence of the instantaneous nonlinear absorption could explain the variety of 2PA-characteristics reported in the literature.

Second, this a-Si:H nanowire shows a significant non-instantaneous amplitude and phase response, with a characteristic lifetime of  $\sim 1.5$  ns. The delayed phase shift is clearly positive, in the same direction as the instantaneous Kerr phase shift, which contradicts what is commonly observed for free-carrier dispersion. We know of one previous publication in which a similar result was documented for an a-Si:H waveguide [2]. But, in that report the effect was much weaker, and the authors attributed it to carriers.

Third, the magnitude of the cross-absorption transient is observed to scale in proportion to  $P_{\text{pump}}P_{\text{probe}}$ . This fact, together with the sign of the non-instantaneous nonlinear phase shift and the absence of two-photon absorption, means the non-instantaneous nonlinearity cannot be attributed to free carrier effects. The power scaling we observe here is similar to that predicted by the two-state absorption model (with the instantaneous two-photon absorption coefficient set to zero) proposed by Ikeda, et al [21]. However, the TSA model attributes the delayed response to free-carrier absorption and dispersion, which is not commensurate with the results we observe.

Phenomenologically, the response we observe is best described as intensity-dependent instantaneous nonlinear refraction coupled with intensity-dependent non-instantaneous nonlinear absorption and refraction. The sign of the nonlinear refraction is positive for the instantaneous and non-instantaneous components. Without further information, we refrain from assigning a particular physical mechanism(s) to the observed phenomena.

We have pointed out that our current work contradicts many previous reports about a-Si:H. For completeness, we note that the results presented here conflict even with a report we ourselves made about nonlinear absorption in an a-Si:H waveguide (a waveguide composed of exactly the same material studied here). In [10], we attributed the observed power-dependent saturation of four-wave-mixing efficiency to two-photon absorption and free-carrier absorption. We now know that the saturation of this continuous-wave process resulted from the delayed

nonlinear absorption we have documented here.

We mention our error because it highlights the difficulty of measuring the nonlinear figure-of-merit of a-Si:H, which depends directly on a measurement of the 2PA coefficient. The 2PA coefficient is typically measured using nonlinear transmission of optical pulses. This is acceptable for instantaneous 2PA, where the nonlinear transmission depends only on the instantaneous power. However, our measurements suggest that the nonlinear absorption in a-Si:H is not instantaneous in nature – rather, it has no instantaneous component. Consequently, the measurement of the 2PA coefficient using short pulses depends non-trivially on the pulse duration and the repetition period, in a way that has not been considered in many of the experimental measurements reported in the literature.

Despite the non-instantaneous nonlinearity, a-Si:H remains very promising for applications, especially pulsed applications where only a fraction of the delayed absorption is sampled by the field. Understanding the fabrication-dependence of the nonlinearity of a-Si:H is an important research goal and we leave it as future work to perform linear spectroscopy of a-Si:H samples fabricated under various conditions. Doing so, we hope to gain insight into the microscopic origins of the nonlinearity in this material and identify paths towards the mitigation of nonlinear losses.

## 7. Conclusion

We employed a range of both quasi-continuous-wave and pulsed measurements to measure the non-instantaneous nonlinear response of an amorphous hydrogenated silicon waveguide, and we compared the response to that of a crystalline silicon waveguide of comparable dimension. Quasi-continuous-wave XPM and XAM measurements reveal that both materials exhibit a nanosecond-scale phase and amplitude nonlinearity. However, at sufficiently high modulation frequencies, the a-Si:H waveguides show a purely refractive nonlinearity, signifying an absence of instantaneous 2PA. Pump-probe measurements were used to further study the magnitude and phase response, and to quantify the power dependence of the non-instantaneous contribution. In all cases, the observations are seen to be inconsistent with an interpretation as free-carrier effects.

These results show that the nature and origin of the non-instantaneous nonlinearity in amorphous-hydrogenated silicon is more complex than is ordinarily assumed for crystalline silicon devices, and that existing models for the nonlinearity must be re-examined before conclusions can be drawn about the suitability and merits of this material for nonlinear optical processing.

## Acknowledgments

Ke-Yao Wang and Amy C. Foster acknowledge support from the DARPA Young Faculty Award Program under award number N66001-12-1-4248.